Synthesis of single-crystal La$_{0.67}$Sr$_{0.33}$MnO$_3$ freestanding films with different crystal-orientation

Zengxing Lu, Jingwu Liu, 🆔 Jiatai Feng, Xuan Zheng, Li-hong Yang, 🆔 Chen Ge, Kui-juan Jin, 🆔 Zhiming Wang, and Run-Wei Li

open access

View Online   Export Citation   CrossMark

ARTICLES YOU MAY BE INTERESTED IN

Aspects of the synthesis of thin film superconducting infinite-layer nickelates
APL Materials 8, 041107 (2020); https://doi.org/10.1063/5.0005103

Preparation and characterization of a flexible ferroelectric tunnel junction
Applied Physics Letters 116, 222904 (2020); https://doi.org/10.1063/5.0006638

Emergent ferromagnetism with tunable perpendicular magnetic anisotropy in short-periodic SrIrO$_3$/SrRuO$_3$ superlattices
Applied Physics Letters 116, 142401 (2020); https://doi.org/10.1063/1.5144643

Synthesis of single-crystal La$_{0.67}$Sr$_{0.33}$MnO$_3$ freestanding films with different crystal-orientation

Zengxing Lu,[1,2] Jingwu Liu,[1,2,3] Jiatai Feng,[1,2] (ID) Xuan Zheng,[1,2,4] Li-hong Yang,[5] Chen Ge,[5] (ID) Kui-juan Jin,[5] Zhiming Wang,[1,2,6,a)] (ID) and Run-Wei Li[1,2,6]

AFFILIATIONS

[1] CAS Key Laboratory of Magnetic Materials and Devices, Ningbo Institute of Materials Technology and Engineering, Chinese Academy of Sciences, Ningbo 315201, China

[2] Zhejiang Province Key Laboratory of Magnetic Materials and Application Technology, Ningbo Institute of Materials Technology and Engineering, Chinese Academy of Sciences, Ningbo 315201, China

[3] Nano Science and Technology Institute, University of Science and Technology of China, Hefei 230026, China

[4] New Materials Institute, The University of Nottingham Ningbo China, Ningbo 315100, China

[5] Beijing National Laboratory for Condensed Matter Physics, Institute of Physics, Chinese Academy of Sciences, Beijing 100190, China

[6] Center of Materials Science and Optoelectronics Engineering, University of Chinese Academy of Sciences, Beijing 100049, China

a) Author to whom correspondence should be addressed: zhiming.wang@nimte.ac.cn

ABSTRACT

We report the synthesis of single-crystal La$_{0.67}$Sr$_{0.33}$MnO$_3$ (LSMO) freestanding films with different crystal orientations. By using pulsed laser deposition, water soluble perovskite-like sacrificial layers Sr$_3$Al$_2$O$_6$ (SAO) followed by LSMO films are grown on differently oriented SrTiO$_3$ substrates. Freestanding LSMO films with different orientations are obtained by etching the SAO in pure water. All the freestanding films show room-temperature ferromagnetism and metallicity, independent of the crystal orientation. Intriguingly, the Curie temperature (T_C) of the freestanding films is increased due to strain relaxation after releasing from the substrates. Our results provide an additional degree of freedom to tailor the properties of freestanding perovskite oxide heterostructures by crystal orientation and an opportunity to further integrate different oriented films together.

Over the last decades, conventional two-dimensional (2D) materials, such as graphene and MoS$_2$, have been widely investigated.[1–4] The 2D material is typically one of the freestanding materials that have an isolated structure resulting in remarkable electronic properties and showing great potential for practical applications.[2,3] Apart from the conventional 2D materials, transition-metal oxide perovskites have also attracted tremendous interest owing to their abundant properties, including multiferroic, superconductivity and colossal magnetoresistance, and have been regarded as one promising candidate for emerging functional materials.[5–8] Therefore, the perovskites are expected to be prepared with freestanding form such

as the 2D materials and further enrich the investigation in physics and functional devices. Indeed, single-crystal freestanding oxide films have been successfully synthesized.[9–12] In 2016, Lu and co-workers[12] developed a method to fabricate high-quality freestanding oxide films and superlattices using water-soluble perovskite-like oxide, Sr$_3$Al$_2$O$_6$ (SAO), as a sacrificial buffer layer. Then, they further explored the two-dimensional limit of the freestanding films.[13] Recently, Ji et al.[14] further prepared ultrathin isolated BiFeO$_3$ films even down to one-unit-cell scale. Super-elastic BaTiO$_3$[15] and super-conductive YBa$_2$Cu$_3$O$_{7-x}$[16] freestanding membranes were also prepared with the same method. At the same time, several prototype

devices based on the freestanding oxide films are prepared and show remarkable functionality, such as the ferroelectric capacitor[17] and resistance switching random memory.[18] These efforts demonstrate that freestanding perovskite films just like the 2D materials can be well fabricated and utilized, playing an important role in both fundamental and device research.

Besides, compared with the 2D materials, perovskite oxides can be synthesized with different crystal orientations. Therefore, the different oriented oxides with freestanding form could be prepared using the sacrificial layer methods, which will provide a new degree to obtain novel properties in freestanding materials. Prior works are focused on fabricating high-quality single-crystal freestanding films on single (001) oriented substrates.[12–18] Little attention is paid to understand whether this technique can be appropriate for fabricating different oriented freestanding films and investigating their corresponding properties. The physical properties are closely related to the crystalline orientation in perovskites. For example, orientation-dependent ferroelectric and magnetic anisotropy were identified in bulk $BiFeO_3$[19] and $SrRuO_3$,[20,21] respectively. More importantly, at the 2D oxide interface where symmetry, surface polarity, and oxygen octahedral coupling differ from the bulk counterpart, the crystalline orientations will have a great impact on the properties of oxide heterostructures.[22–24] For instance, Gibert et al.[25] found a large exchange bias in (111)-oriented $LaNiO_3$–$LaMnO_3$ superlattices, which was absent in the (001) sample, while Catalano et al.[26]

observed an orientation-dependent metal–insulator transition in $NdNiO_3$ thin films. Therefore, it is important to investigate synthesis of TMO freestanding film with different crystal-orientations and explore their novel properties.

In this Letter, we report the synthesis of single-crystal $La_{0.67}Sr_{0.33}MnO_3$ (LSMO) freestanding films with (001), (110), and (111) orientations. The freestanding film was fabricated by the method of dissolving the water-soluble SAO buffer layer. Then, the LSMO freestanding films were achieved with the assistance of polyimide (PI) tape. By measuring their magnetic and electrical behaviors, we find that all of the different oriented films show the room-temperature ferromagnetic and metallic behaviors before and after being released, independent of the crystal orientation.

As shown in Fig. 1(a), the hydrogarnet SAO is a perovskite-like oxide. It has a cubic structure with a lattice constant a = 15.844 Å.[12] Its constant is about four times compared with the popular perovskites, including substrate $SrTiO_3$ (STO, a_{STO} = 3.905 Å, 4 × a_{STO} = 15.620 Å).[12] Viewed on three typical planes, i.e., (001), (110) and (111) shown in Figs. 1(b)–1(d), each unit cell of the SAO has an area of a^2, $\sqrt{2}a^2$, and $\sqrt{3}a^2$, respectively. For the three planes of the STO, it is a_{STO}^2, $\sqrt{2}a_{STO}^2$, and $\sqrt{3}a_{STO}^2$, respectively. Therefore, one unit cell of SAO can accommodate 4 × 4 STO unit cells well in any plane. That is the same for the bulk LSMO (a_{LSMO} = 3.87 Å) too.[27] Such a lattice matching relationship is the precondition of preparing single-crystal freestanding films with various orientations.
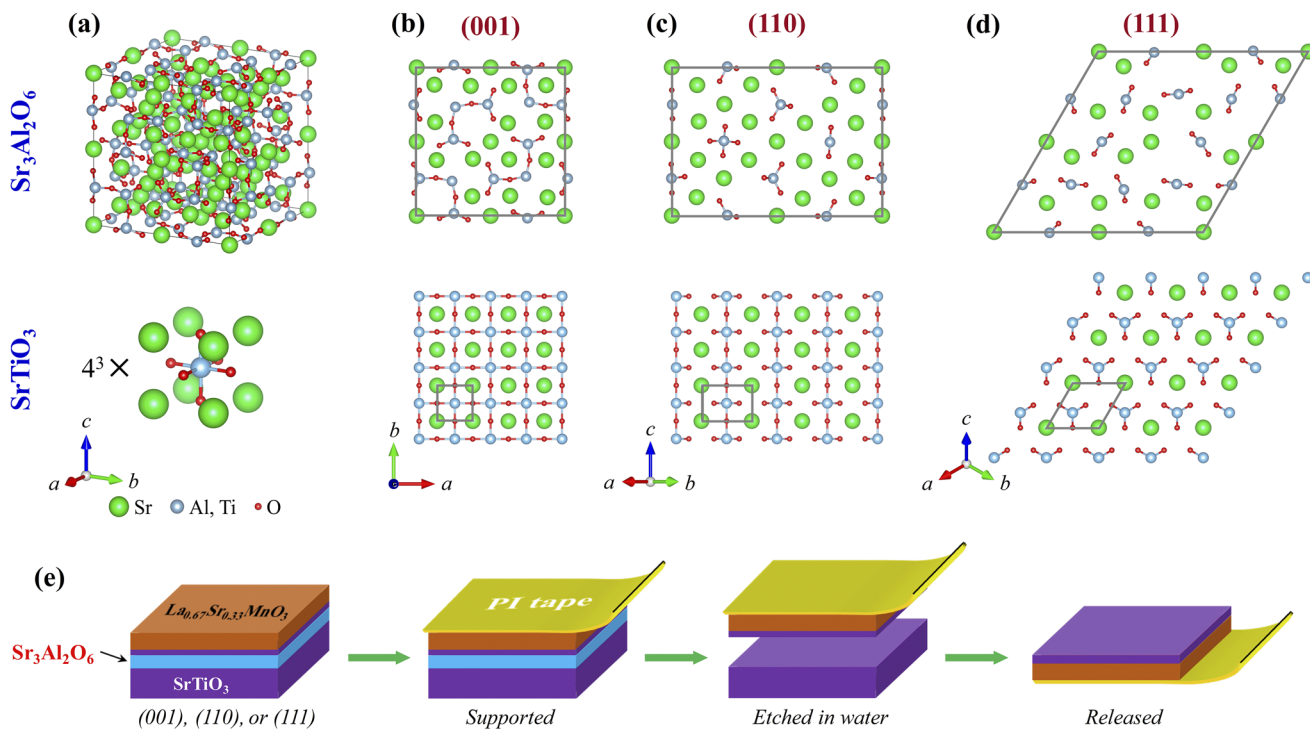
FIG. 1. Synthesis of freestanding $La_{0.67}Sr_{0.33}MnO_3$ (LSMO) films with (001), (110), and (111) crystal orientations. (a) Cubic lattice structures of SAO and STO and their matching relationship viewed on (b) (001), (c) (110), and (d) (111) planes. Gray frames indicate primitive 2D unit cells on different planes. One 2D unit cell of SAO matches 4 × 4 unit cells of STO projected onto three different planes. (e) Synthesis of different oriented freestanding LSMO films, including heterostructure growth, and oxide membrane release and transfer. PI is the abbreviation of polyimide tape.

Hence, in this work, we epitaxially deposit SAO/STO/LSMO heterostructures on the STO substrates by pulsed laser deposition (PLD). Before growth, the substrates are annealed at 850 °C in the PLD chamber for 30 min to achieve a smooth surface with well-defined step-and-terrace morphology. After that, there are extra STO with several unit cells deposited on the substrates to eliminate possible surface reconstruction. Then, the SAO layer is deposited on the STO substrates at a substrate temperature T_{sub} = 700 °C with an oxygen pressure Po_2 = 1×10^{-3} mbar and a laser fluence of 1.3 J/cm^2. During the growth, reflection high-energy electron diffraction (RHEED) was used to monitor the thicknesses and surface quality of SAO deposited on different substrates. The deposition condition for the SAO layer on (001) STO was carefully optimized to achieve layer-by-layer growth, and the thickness was controlled with 6 unit cells (Fig. S1a). The (110) and (111) SAO were deposited with identical pulse counts. The RHEED patterns taken in vacuum after growth of the three SAO layers are shown in Figs. S2(d)–2S(f). The clear streaks and 2D spots reveal that the SAO layers are grown in 2D growth mode and have a smooth

surface and high-quality crystallization. It indicates that the SAO can be epitaxially deposited on STO substrates well along aforementioned orientations.

Based on the epitaxial SAO layers, 3-unit-cell STO buffer layers and 80-unit-cell LSMO films are successively grown. The STO layers are used to prevent cation diffusion between SAO and LSMO, which has been found in previous work.[28] At first, they are grown on (001) STO with the same laser fluence (1.3 J/cm^2) at T_{sub} = 700 °C and Po_2 = 0.1 mbar. Judging from the RHEED oscillating curve (Fig. S1b), the LSMO film was optimized to grow in the layer-by-layer mode too. Its thickness was controlled with 80 unit cells. Next, the (110) and (111) films were deposited with identical pulse counts. It should be noted that the T_{sub} for (110) and (111) LSMO depositing is optimized at 600 °C to reduce the influence due to the surface polarity of the substrates and obtain smooth films.[23] Finally, these heterostructures are immersed in pure water and etch the SAO to separate the LSMO films from the substrates, as shown in Fig. 1(e). During the process, polyimide (PI) tape is used as a support to achieve continuous and complete films. This is beneficial to prevent fragmenting
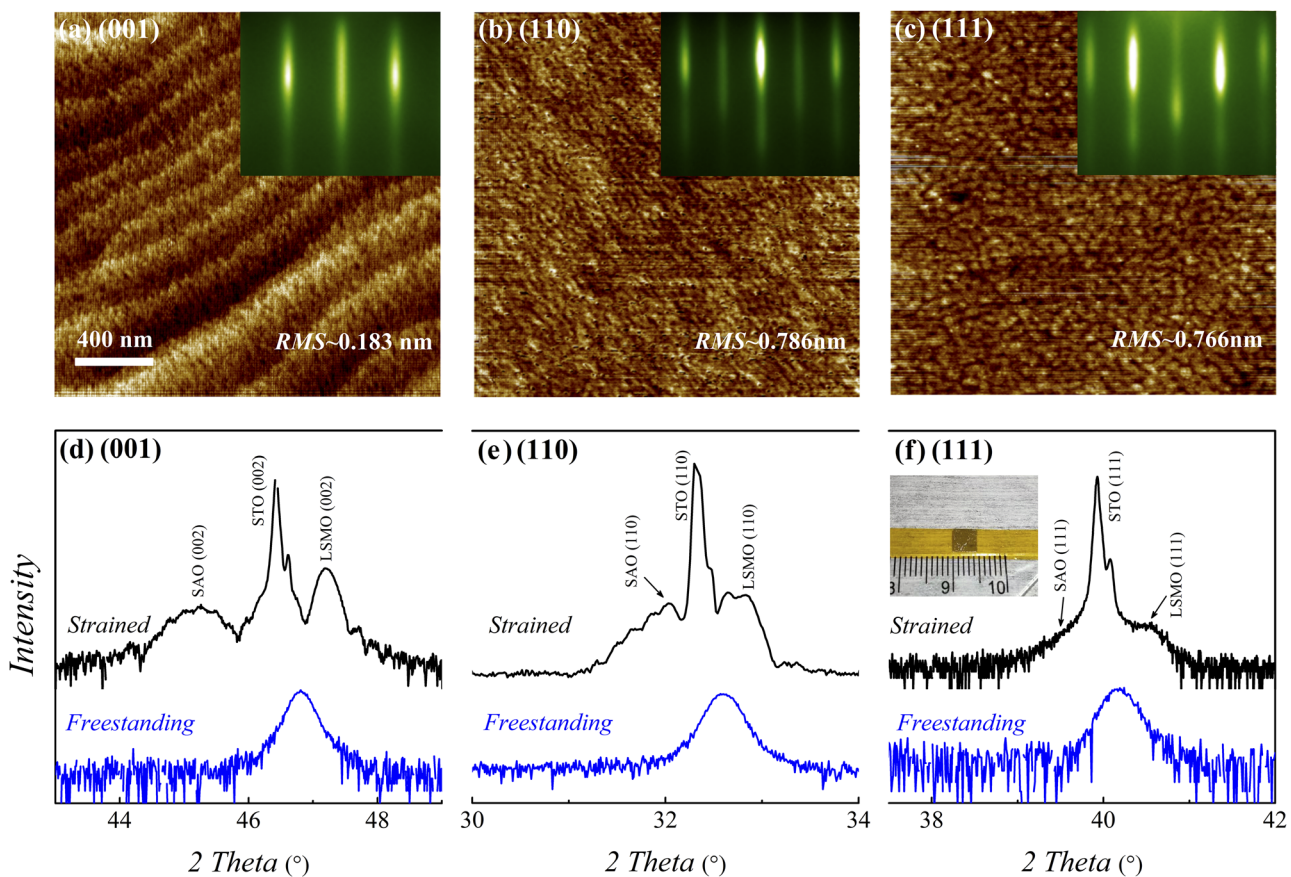
FIG. 2. Epitaxial growth and surface morphology of different oriented La$_{0.67}$Sr$_{0.33}$MnO$_3$ (LSMO). AFM images of strained LSMO films with (a) (001), (b) (110), and (c) (111) crystal orientations. Insets show the RHEED patterns of the films grown with different crystalline orientations. XRD 2θ-ω scans of the strained and freestanding LSMO films with (d) (001), (e) (110), and (f) (111) orientations. Inset in (f) shows the optical photograph of the transferred LSMO film. The gray area is the freestanding LSMO film exfoliated from the STO substrate. rms is the abbreviation of root-mean-square of roughness.

the film in the case of directly lifting off without supporting layer or with the assistance of a cover layer such as polymethyl methacrylate or polystyrene.[9]

Figure 2 illustrates the sample quality of strained LSMO films epitaxially deposited on STO substrates with different orientations including (001), (110), and (111). The atomic force microscopy (AFM) and RHEED are used to characterize the surface and crystallization quality of the three strained films. Figures 2(a)–2(c) show the surface morphology of different oriented LSMO films. Atomically flat (001) LSMO surfaces are obtained with the clear terrace-and-step, as shown in Fig. 2(a) (with a roughness of 0.183 nm), while (110) and (111) oriented films have the roughness of 0.786 nm and 0.766 nm [Figs. 2(b) and 2(c)], respectively, proving that these films host the smooth surface. Furthermore, as shown in the insets, the clear streaks and 2D spots in RHEED patterns reveal that the films were grown in 2D growth mode. After the films are exfoliated from the substrate, the surface of freestanding films remains smooth, as shown in Figs. S3(a)–S3(c). To further characterize the crystalline quality, we preformed XRD θ–2θ scans on both strained and released films, as shown in Figs. 2(d)–2(f). The main peaks, i.e., (00l), (hk0), and (hkl), of the SAO and LSMO corresponding to the indices of the substrate are observed, revealing the epitaxial growth and single phase. These confirm the high-quality deposition of our films. Then, we etch the heterostructures following the process motioned above and obtain the freestanding LSMO films. By analyzing the scans of the freestanding films, we found that the LSMO peaks shift

to the left compared the strained films. Correspondingly, their interplanar distances (d) are determined as 3.88 Å, 2.75 Å, and 2.24 Å along (001), (110), and (111) directions, respectively, matching the relationship of d_{001}: d_{110}: d_{111} = 1:$\frac{\sqrt{2}}{2}$:$\frac{\sqrt{3}}{3}$ well. Moreover, these values are close to the parameters of the bulk LSMO,[27,29] indicating a fully relaxed films after lift-off. So far, we have successfully fabricated freestanding single crystal LSMO films with three different orientations.

Next, we explored the magnetic and electrical properties of strained and freestanding films with different orientations. The measurements of hysteresis loops (M–H loops) and temperature-dependent magnetization (M–T curves) were performed. Figures 3(a)–3(c) illustrate the M–H loops with applied in-plane magnetic field for (001), (110), and (111) LSMO films. All of the strained and freestanding films have a saturate moment (M_S) with 3.48 μ_B, which is close to the value reported in Ref. 30, indicating the high quality of the films, while the (110) film has the highest coercive filed (H_C) and residual moments (M_rs) compared with (001) and (111) films according to the M–H loops. These orientation-dependent loops indicate that the crystalline orientation can influence the magnetism of the LSMO film. After release, the ferromagnetism is preserved well in each oriented film. Figures 3(d)–3(f) show the temperature dependence of magnetization. All of the strained and freestanding films show room temperature ferromagnetism. We note the Curie temperature (T_C) of all films is increased after lift-off. It changes from 307 K to 321 K, from 318 K to 329 K, and from 343 K
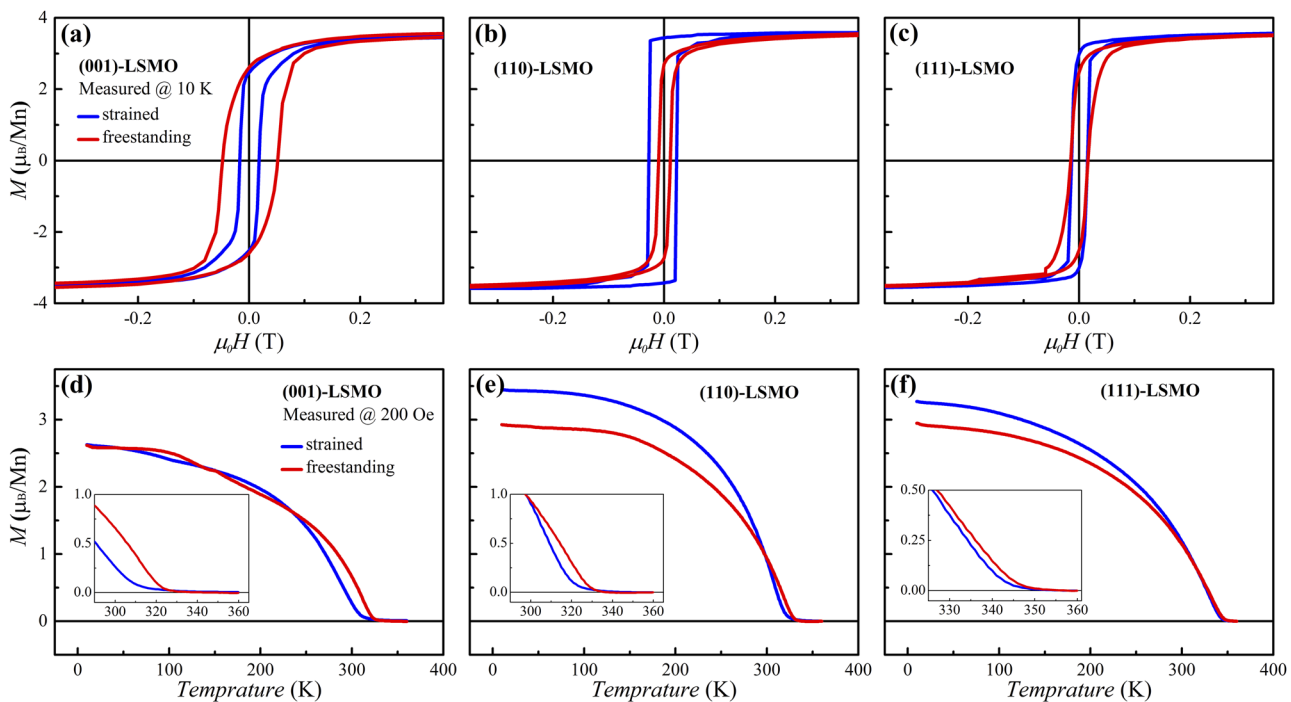

FIG. 3. Magnetic properties of different oriented La$_{0.67}$Sr$_{0.33}$MnO$_3$ (LSMO) before and after release. (a) Schematics of the transport measurements in the strained and freestanding films. Magnetization loops (M–H loops) of (a) (001) LSMO, (b) (110) LSMO, and (c) (111) LSMO films before (blue) and after (red) exfoliated from the substrates. Temperature-dependent magnetization (M–T curves) of (d) (001) LSMO, (e) (110) LSMO, and (f) (111) LSMO films before (blue) and after (red) release. Insets are the magnified plots showing the M–T curves. The M–H loops were measured at 10 K. The M–T curves were measured at 200 Oe.

to 346 K for the (001)-, (110)-, and (111)-oriented films, respectively. This enhancement can be contributed to the strain relaxation in the released films [Figs. 2(d)–2(f)], which affects the Mn–O–Mn bonding environments.[31,32] These variations reveal that the orientation and stress release can modulate the magnetism to a degree.

To reveal the electrical properties of the oriented film before and after being transferred, the temperature dependence of resistivity was measured in the strained and freestanding LSMO films. As shown in Figs. 4(a)–4(c), a metallic behavior is observed in the strained films and kept well in the freestanding films. Therefore, these films are room-temperature ferromagnetic metals regardless of the orientation and stress. However, we find that the resistivity (ρ) is enhanced after being released for every oriented film. This is due to the cracks generated during the transfer process, as shown in Fig. S3d. Additionally, around the T_C temperature, the (111) freestanding LSMO film shows a metal–insulator transition behavior, which is not observed in the other films. These results indicate that electric properties of the LSMO film can be modulated by the crystalline orientation and strain relaxation.

It has been widely recognized that the use of the water-soluble sacrificial layer presents a general approach to synthesize single-crystal freestanding oxide films.[12–16] Some advantages of this freestanding technique can be predicted, such as the reusability of

perovskite substrates,[12,16] the ability to grow freestanding metal films and prepare flexible oxide-based electronic devices.[15,18] Our study demonstrates that the technique can be utilized for producing the oxide membranes with different orientations. This provides an additional degree of freedom to tailor the properties of freestanding perovskite oxide heterostructures using crystal orientation. Moreover, one can further integrate differently oriented films together to explore novel physics and chemistry properties and develop emerging functional devices.

In summary, we have epitaxially grown high-quality LSMO films on SAO-coated STO substrates with various crystal orientations. By comparing the magnetic and electric characterizations of the oriented films, they are room-temperature ferromagnetic metals. With the assistance of the PI tape, we obtain single-crystal LSMO freestanding films with different orientations by dissolving the SAO layer. We find that the T_C of freestanding films is increased in freestanding films due to strain relaxation after being released from the substrates. These demonstrate that inserting a sacrificial layer is a feasible way to prepare the single-crystal freestanding perovskite film with different crystal orientations. Our results provide the opportunity for further tailoring the properties of freestanding perovskite oxide heterostructures by crystal orientation and integrating different oriented films together.
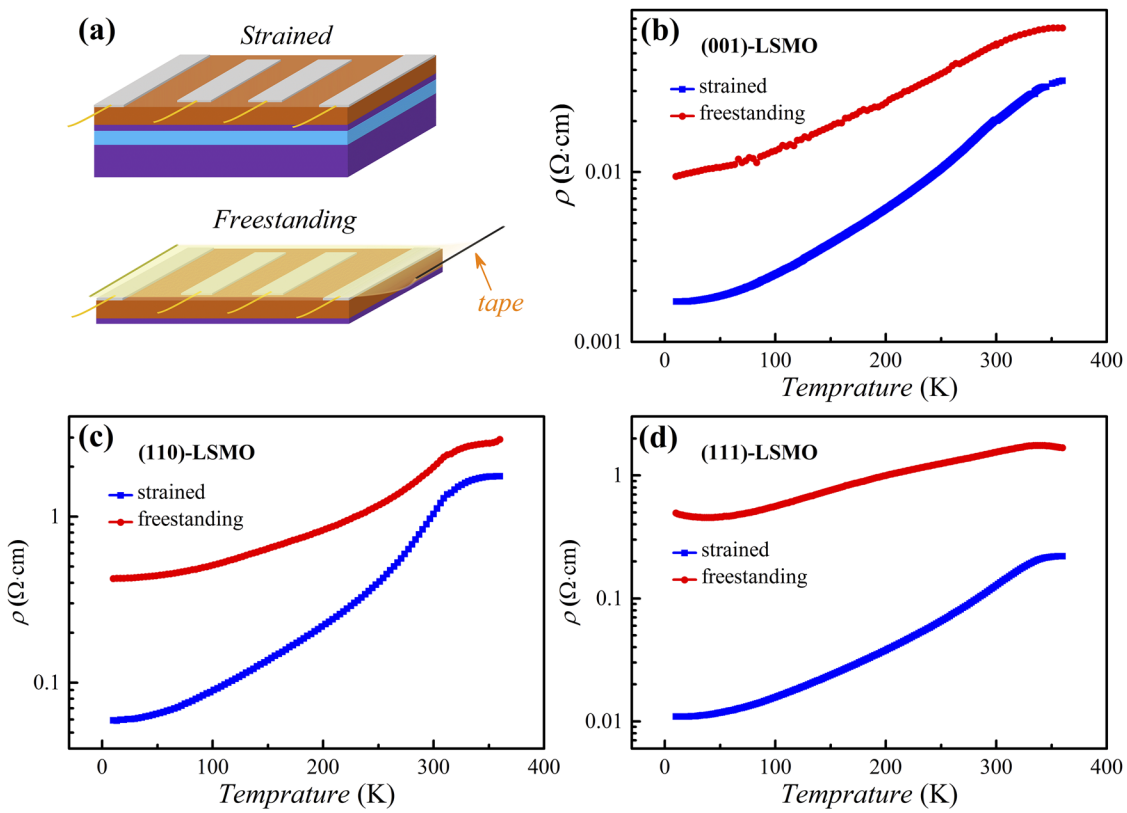

FIG. 4. Electrical properties of different oriented La$_{0.67}$Sr$_{0.33}$MnO$_3$ (LSMO) before and after release (a). Temperature-dependent resistivity (ρ–T curves) of (b) (001) LSMO, (c) (110) LSMO, and (d) (111) LSMO before (blue) and after (red) released from the substrate.

See the supplementary material for the growth of $Sr_3Al_2O_6$/ $SrTiO_3$/$La_{0.67}Sr_{0.33}MnO_3$ (SAO/STO/LSMO) heterostructures deposited on the (001)-, (110)-, and (111)-oriented STO substrates, including RHEED patterns of the annealed STO substrates and as-grown SAO layers (Fig. S1), RHEED intensity oscillations of (001)-SAO and LSMO layers (Fig. S2), the fabricating process of the free-standing films, and the characterization of crystallization and surface quality and magnetic and electric properties.

REFERENCES

[1] K. S. Novoselov, A. K. Geim, S. V. Morozov, D. Jiang, Y. Zhang, S. V. Dubonos, I. V. Grigorieva, and A. A. Firsov, Science **306**, 666 (2004).

[2] M. Xu, T. Liang, M. Shi, and H. Chen, Chem. Rev. **113**, 3766 (2013).

[3] S. Z. Butler, S. M. Hollen, L. Cao, Y. Cui, J. A. Gupta, H. R. Gutiérrez, T. F. Heinz, S. S. Hong, J. Huang, A. F. Ismach, E. Johnston-Halperin, M. Kuno, V. V. Plashnitsa, R. D. Robinson, R. S. Ruoff, S. Salahuddin, J. Shan, L. Shi, M. G. Spencer, M. Terrones, W. Windl, and J. E. Goldberger, ACS Nano **7**, 2898 (2013).

[4] M. Yankowitz, Q. Ma, P. Jarillo-Herrero, and B. J. LeRoy, Nat. Rev. Phys. **1**, 112 (2019).

[5] R. Ramesh and N. A. Spaldin, Nat. Mater. **6**, 21 (2007).

[6] Y. Tokura, M. Kawasaki, and N. Nagaosa, Nat. Phys. **13**, 1056 (2017).

[7] N. A. Spaldin, S.-W. Cheong, and R. Ramesh, Phys. Today **63**(10), 38 (2010).

[8] S. Yamada, N. Abe, H. Sagayama, K. Ogawa, T. Yamagami, and T. Arima, Phys. Rev. Lett. **123**, 126602 (2019).

[9] L. Shen, L. Wu, Q. Sheng, C. Ma, Y. Zhang, L. Lu, J. Ma, J. Ma, J. Bian, Y. Yang, A. Chen, X. Lu, M. Liu, H. Wang, and C.-L. Jia, Adv. Mater. **29**, 1702411 (2017).

[10] S. R. Bakaul, J. Kim, S. Hong, M. J. Cherukara, T. Zhou, L. Stan, C. R. Serrao, S. Salahuddin, A. K. Petford-Long, D. D. Fong, and M. V. Holt, Adv. Mater. **32**, 1907036 (2019).

[11] D. M. Paskiewicz, R. Sichel-Tissot, E. Karapetrova, L. Stan, and D. D. Fong, Nano Lett. **16**, 534 (2016).

[12] D. Lu, D. J. Baek, S. S. Hong, L. F. Kourkoutis, Y. Hikita, and H. Y. Hwang, Nat. Mater. **15**, 1255 (2016).

[13] S. S. Hong, J. H. Yu, D. Lu, A. F. Marshall, Y. Hikita, Yi Cui, and H. Y. Hwang, Sci. Adv. **3**, 5173 (2017).

[14] D. Ji, S. Cai, T. R. Paudel, H. Sun, C. Zhang, L. Han, Y. Wei, Y. Zang, M. Gu, Y. Zhang, W. Gao, H. Huyan, W. Guo, D. Wu, Z. Gu, E. Y. Tsymbal, P. Wang, Y. Nie, and X. Pan, Nature **570**, 87 (2019).

[15] G. Dong, S. Li, M. Yao, Z. Zhou, Y.-Q. Zhang, X. Han, Z. Luo, J. Yao, B. Peng, Z. Hu, H. Huang, T. Jia, J. Li, W. Ren, Z.-G. Ye, X. Ding, J. Sun, C.-W. Nan, L.-Q. Chen, J. Li, and M. Liu, Science **366**, 475 (2019).

[16] Z. Chen, B. Y. Wang, B. H. Goodge, D. Lu, S. S. Hong, D. Li, L. F. Kourkoutis, Y. Hikita, and H. Y. Hwang, Phys. Rev. Mater. **3**, 060801(R) (2019).

[17] S. R. Bakaul, C. R. Serrao, O. Lee, Z. Lu, A. Yadav, C. Carraro, R. Maboudian, R. Ramesh, and S. Salahuddin, Adv. Mater. **29**, 1605699 (2017).

[18] D. Lu, S. Crossley, R. Xu, Y. Hikita, and H. Y. Hwang, Nano Lett. **19**, 3999 (2019).

[19] S.-H. Baek, C. M. Folkman, J.-W. Park, S. Lee, C.-W. Bark, T. Tybell, and C.-B. Eom, Adv. Mater. **23**, 1621 (2011).

[20] C. U. Jung, H. Yamada, M. Kawasaki, and Y. Tokura, Appl. Phys. Lett. **84**, 2590 (2004).

[21] L. Liu, Q. Qin, W. Lin, C. Li, Q. Xie, S. He, X. Shu, C. Zhou, Z. Lim, J. Yu, W. Lu, M. Li, X. Yan, S. J. Pennycook, and J. Chen, Nat. Nanotech. **14**, 939 (2019).

[22] Y. Tang, Y. Zhu, X. Ma, Z. Hong, Y. Wang, W. Wang, Y. Xu, Y. Liu, B. Wu, L. Chen, C. Huang, L. Chen, Z. Chen, H. Wu, and S. J. Pennycook, Adv. Funct. Mater. **29**, 1901687 (2019).

[23] M. Saghayezhian, L. Chen, G. Wang, H. Guo, E. W. Plummer, and J. Zhang, Phys. Rev. B **93**, 125408 (2016).

[24] A. Biswas, P. B. Rossen, C.-H. Yang, W. Siemons, M.-H. Jung, I. K. Yang, R. Ramesh, and Y. H. Jeong, Appl. Phys. Lett. **98**, 051904 (2011).

[25] M. Gibert, P. Zubko, R. Scherwitzl, J. Iniguez, and J.-M. Triscone, Nat. Mater. **11**, 195 (2012).

[26] S. Catalano, M. Gibert, V. Bisogni, F. He, R. Sutarto, M. Viret, P. Zubko, R. Scherwitzl, G. A. Sawatzky, T. Schmitt, and J.-M. Triscone, APL Mater. **3**, 062506 (2015).

[27] F. Tsui, M. C. Smoak, T. K. Nath, and C. B. Eom, Appl. Phys. Lett. **76**, 2421 (2000).

[28] D. J. Baek, D. Lu, Y. Hikita, H. Y. Hwang, and L. F. Kourkoutis, APL Mater. **5**, 096108 (2017).

[29] A. Hammouche, E. Siebert, and A. Hammou, Mater. Res. Bull. **24**, 367 (1989).

[30] A. Urushibara, Y. Moritomo, T. Arima, A. Asamitsu, G. Kido, and Y. Tokura, Phys. Rev. B **51**, 14103 (1995).

[31] F. Yang, N. Kemik, M. D. Biegalski, H. M. Christen, E. Arenholz, and Y. Takamura, Appl. Phys. Lett. **97**, 092503 (2010).

[32] Y. Takamura, R. V. Chopdekar, E. Arenholz, and Y. Suzuki, Appl. Phys. Lett. **92**, 162504 (2008).